

Multi-scale finite element analysis of acoustic waves using global residual-free meshfree enrichments

C.T. Wu* and Wei Hu

Livermore Software Technology Corporation, 7374 Las Positas Road, Livermore, CA 94551, USA

(Received March 1, 2013, Revised April 8, 2013, Accepted May 5, 2013)

Abstract. In this paper, a multi-scale meshfree-enriched finite element formulation is presented for the analysis of acoustic wave propagation problem. The scale splitting in this formulation is based on the Variational Multi-scale (VMS) method. While the standard finite element polynomials are used to represent the coarse scales, the approximation of fine-scale solution is defined globally using the meshfree enrichments generated from the Generalized Meshfree (GMF) approximation. The resultant fine-scale approximations satisfy the homogenous Dirichlet boundary conditions and behave as the “global residual-free” bubbles for the enrichments in the oscillatory type of Helmholtz solutions. Numerical examples in one dimension and two dimensional cases are analyzed to demonstrate the accuracy of the present formulation and comparison is made to the analytical and two finite element solutions.

Keywords: acoustic; multi-scale; finite element; Helmholtz; meshfree

1. Introduction

There are many important scientific and engineering problems that involve dealing with information on multiple spatial and temporal scales. The time-harmonic acoustics governed by the Helmholtz equation in structural acoustics and electromagnetic applications is one of such problems which require simultaneous resolution of different scales spanned over a wide frequency spectrum. In particular, evanescent waves play a significant role in the design of various nano-optical and nano-biological sensors, and thus demand advanced modeling technique because of their multi-scale nature. Numerical analysis by the standard finite element method of such problems in the medium or higher frequency regimes is either computationally unfeasible or simply unreliable, particularly in the presence of evanescent waves. This is because the standard low-order continuous Galerkin finite element method fails to adequately control numerical dispersion errors (Belytschko and Mullen 1978) when the wave number increases. As a consequence, the finite element method not only inaccurately approximates the oscillatory part of the solution, but also experiences a notorious pollution error (Ihlenburg and Babuska 1995), a numerical error related to the phase difference between the exact and finite element solutions. To minimize the pollution error and obtain an accurate solution in the finite element analysis of Helmholtz equation, the resolution of mesh should be adjusted to the wave number according to

*Corresponding author, Ph.D., E-mail: ctwu@lstc.com

the “rule of thumb” (Harari and Hughes 1991). In addition to the hierarchical p-refinement of finite element method (Ihlenburg and Babuska 1997), many non-standard finite element methods have been developed in the past two decades to reduce the pollution error. They include Galerkin/Least Squares (GLS) method (Harari and Hughes 1992), Generalized Finite Element Method (Babuska *et al.* 1995), Discontinuous Galerkin Method (Farhat *et al.* 2001) and Bubble-based Stabilization Method (Harari and Gosteev 2007). Recent developments in Variational Multi-scale (VMS) Method (Hughes *et al.* 2004, Harari 2008) have shown that several non-standard finite element methods are closely related to VMS method. A common assumption in those methods is to consider the fine-scale enrichments to vanish on the inter-element boundaries, thus localizing the effect of the fine-scale. The obvious limitation associated with the loss of essential global effects inherent in local approaches may be overcome by including the inter-element jump terms (Oberai and Pinsky 2000) in the residual-based stabilized finite element method or employing nonconforming methods (Franca *et al.* 2005) under the Petrov-Galerkin framework. The early developments of multi-scale methods for Helmholtz equation were based on the element fine-scale Green functions (Oberai and Pinsky 1998, Hughes *et al.* 2004). In general, the element fine-scale Green functions become increasingly complicated (Hughes and Sangalli 2007) as the order of the coarse-scale space is increased. More recently, a variational multi-scale method (Baiges and Codina 2013) was proposed to include the contribution of the fine-scale by imposing the continuity of fluxes across the inter-element boundaries. Similar to the approach in the GLS method, the stabilization parameter associated with the inter-element boundary terms in VMS method is determined by a dispersion analysis but the VMS method yields a result that is less dependent on the direction of the wave propagation and mesh orientation.

On the other hand, several meshfree formulations (Uras *et al.* 1997, Suleau and Bouillard 2000) have also been developed to solve the wave and Helmholtz equations. It has been shown (Bouillard and Suleau 1998, You *et al.* 2002) that the dispersion and pollution phenomena affect the meshfree and finite element solutions in a similar way. However, the meshfree methods are more accurate than the finite element methods under same discretization (Bouillard and Suleau 1998, Voth and Christon 2001). In comparison with the standard finite element method, the characteristics of mesh-independent and wave-based approximation effectively make the meshfree methods attractive alternative numerical techniques for modeling the acoustic wave propagation problems. Conventional meshfree approximations such as Moving Least-Squares (MLS) approximation (Belytschko *et al.* 1994) and Reproducing Kernel (RK) approximation (Liu *et al.* 1995) do not satisfy the Kronecker-delta property at the boundary thus require special treatments such as Lagrange multiplier to impose the essential boundary conditions. However the method of Lagrange multiplier involves more unknowns which may result in an indefinite discrete linear system and pollute the numerical solution. Other meshfree interpolation methods based on radial point interpolation (Wenterodt and von Estorff 2009) or radial basis functions (Lai *et al.* 2010) were also developed for the analysis of Helmholtz equation and significant accuracy improvements have been made in particular for the medium and high frequency modes. While such methods provide high fidelity predictions of the propagation properties in waveguides, the issues of high conditioning, irregular nodal distribution and boundary effect due to the characteristics of non-locality and over-determined system of equations in those methods have not yet been fully investigated.

Recently a novel approximation scheme, the generalized meshfree (GMF) approximation method (Wu and Koishi 2009, Wu *et al.* 2011), was developed to enhance the smoothness of the approximation as well as to generate the desired weak Kronecker-delta property (Wu and Koishi

2009) at the boundary. The meshfree convex approximation (non-negative and reproducing exactly affine functions) generated by GMF approximation method was shown to be insensitive to the nodal support size in solving the elastostatic problems. Park *et al.* (Park *et al.* 2011) embarked on a detailed dispersion analysis for GMF approximation method and revealed that meshfree convex approximation exhibits smaller lagging phase and amplitude errors than non-convex meshfree approximation in full-discretization of the wave equation. An immersed meshfree Galerkin formulation (Wu *et al.* 2013) was proposed using the nonconforming GMF approximations to solve the interface constraint problems in the composites and was shown to satisfy an optimal error estimates in the energy norm. By incorporating a local meshfree convex approximation into a low-order finite element, an enriched finite element formulation (Wu *et al.* 2012) was developed for solving the linear and nonlinear problems (Hu *et al.* 2012, Wu and Koishi 2012) involving material incompressibility. Their numerical inf-sup study (Wu and Hu 2011) has indicated the pair of spaces in displacements and pressure fields is inf-sup stable. This paper presents another application of meshfree convex approximation in solving the acoustic wave propagation problems. Different from the finite element enrichment using the local meshfree convex approximations for incompressible problems, the fine-scale finite element enrichment in the variational multi-scale method for acoustic wave propagation problems is constructed using the global meshfree convex approximations.

This paper is organized as follows: In Section 2 the basic equation in acoustic wave propagation problem and its variational formulation are reviewed. Section 3 overviews the variational multi-scale formulation and introduces the global residual-free fine-scale enrichments using convex meshfree approximations to the variational multi-scale formulation for analysis of Helmholtz equation. The global fine-scale approximations constructed using the meshfree convex approximations are presented in Section 4. The relationship between the present global fine-scale approximations and the Green's functions is also discussed in the same Section. Two numerical examples are given in Section 5. Final conclusions are made in Section 6.

2. Interior Helmholtz equation

The propagation of pressure waves in an acoustic media inside a domain Ω is governed by the wave equation, which can be derived using the balance of mass, moment and the ideal gas law. Assumed that the state variables pressure P , density ρ and velocity v experience only small harmonic perturbation, then the wave equation can be transformed to the frequency domain and solved by the following Helmholtz equation: Find $p: \Omega \rightarrow \mathcal{C}$

$$\Theta p := -\nabla^2 p - k^2 p = f \quad \text{in } \Omega \tag{1}$$

$$p = p_0 \quad \text{on } \Gamma_D, \tag{2}$$

$$\nabla p \cdot \mathbf{n} = -i\rho\omega v_n \quad \text{on } \Gamma_N \tag{3}$$

$$\nabla p \cdot \mathbf{n} = -i\rho\omega A_n p \quad \text{on } \Gamma_B \tag{4}$$

where Θ denotes the self-adjoint, indefinite, Helmholtz operator. $i = \sqrt{-1}$, $k = \omega/c$ denotes the

wave number and is defined by the ratio between the angular frequency ω and the speed of sound c . p is the complex amplitude of the sound pressure and f is the source term. The boundary consists of three disjointed parts, i.e.,

$$\Gamma = \Gamma_D \cup \Gamma_N \cup \Gamma_B \quad (5)$$

where Γ_D, Γ_N and Γ_B are Dirichlet, Neumann and Robin boundaries respectively. \mathbf{n} is the exterior unit normal vector and v_n stands for the excitation by the vibrating panels on Neumann boundary. A_n is the admittance coefficient that models the structural damping on the Robin boundary. Different from the wave equation which is a linear hyperbolic equation, the Helmholtz equation is also called the reduced wave equation and is a prototype of a linear elliptic equation.

The corresponding variational form of this problem consists of finding

$$p \in V = H_D^1(\Omega) = \{p \in H^1(\Omega) | p = p_0 \text{ on } \Gamma_D\} \text{ such that}$$

$$\int_{\Omega} \nabla w \cdot \nabla p d\Omega - k^2 \int_{\Omega} w p d\Omega + i\rho\omega A_n \int_{\Gamma_B} w p d\Gamma = \int_{\Omega} f w d\Omega - i\rho\omega \int_{\Gamma_N} w v_n d\Gamma \quad \forall w \in H_0^1(\Omega) \quad (6)$$

or in abstract form

$$A(w, p) + i\rho\omega A_n (w, p)_{\Gamma_B} = (w, f)_{\Omega} - i\rho\omega (w, v_n)_{\Gamma_N} \quad \forall w \in H_0^1(\Omega) \quad (7)$$

where $H_0^1(\Omega) = \{w \in H^1(\Omega) | w = 0 \text{ on } \Gamma_D\}$ is the space of kinematically homogeneous test function w . (\cdot, \cdot) is the L_2 inner product. The sesquilinear form $A(w, p)$ is defined by

$$A(w, p) = (\nabla w, \nabla p)_{\Omega} - k^2 (w, p)_{\Omega} \quad (8)$$

Generally speaking, the solution of Helmholtz equation is highly oscillatory at high wave number. Consequently, the discretization in finite element method using the low-order elements has to be fine enough to resolve the oscillatory part of the solution. In another words, fine mesh is needed in order to avoid the loss of stability of the Helmholtz operator Θ , or equivalently to avoid the loss of ellipticity of Helmholtz equation at high wavenumber, i.e., for high wave number k ,

$$A(w_h, w_h) = \|\nabla w_h\|^2 - k^2 \|w_h\|^2 > 0 \quad \forall w_h \in V_h \quad (9)$$

An engineering criterion for the mesh size h to resolve the oscillatory part of the solution is to follow the ‘‘rule of thumb’’ (Harari and Hughes 1991) defined by

$$hk = \text{constant}. \quad (10)$$

Sharp error estimations have been obtained under the small magnitude assumption of hk and have been shown (Ihlenburg and Babuska 1997) that the relative error of the low-order finite element solution in the H_1 -seminorm satisfies

$$\left(\int_{\Omega} |p_h - p|^2 d\Omega \right)^{1/2} \leq (C_1 + C_2 k)(hk)^2 \quad (11)$$

where C_1 and C_2 are constants independent of the wavenumber and element size. The first term on the high-hand side of Eq. (11) represents the usual approximation error. The error in second term dominated the whole errors at medium and high wave numbers. This error is often referred to as a “pollution error” (Ihlenburg and Babuska 1995) which is related to the loss of numerical stability in short wave problems. In essence, the pollution error is associated with the unresolved part of the solution that lies outside the resolution capacity of a given mesh.

3. Variational multi-scale method

As pointed out in last section, the numerical instability in modeling the problem (1)-(4) comes from the inability to measure the effect of unresolved fine-scales at the resolved discretization level. In order to better approximate the oscillatory part of the Helmholtz solution using low-order finite element method, fine-scale solution is introduced via VMS method (Hughes *et al.* 2004, Harari 2008). In the definition of VMS, the exact solution is interpreted as an overlapping of a resolved coarse-scale component and an unresolvable fine-scale component. In frequency domain, the coarse-scale solution corresponds to the combination of frequency modes of lower wave numbers and the fine-scale solution corresponds to the part superimposed by the short wave modes.

Recall the original variational formulation in (6), any $w_h \in H_0^1$ admits a unique decomposition as

$$w_h = w_c + w_f, \text{ with } w_c \in V_c, w_f \in V_f \tag{12}$$

where w_c represent the coarse-scale test functions, and w_f are the fine-scale test functions. The above definition induces a multi-scale decomposition for the function space of the form

$$V_h = V_c \oplus V_f \tag{13}$$

where $V_c \subset V_h$ is the finite-dimensional space obtained through a finite element discretization and V_f is the space of fine-scale functions. Theoretically, V_f does not pose scaling information, and therefore it is infinite-dimensional. However, in the discrete case, V_f can be replaced with various possible finite-dimensional approximations either using analytical methods such as element Green’s functions or numerical methods such as bubbles, hierarchical shape functions, or wavelets. The approximation p_h to the sound pressure p can also be decomposed into two scales.

$$p_h = p_c + p_f \tag{14}$$

Here, $p_c \in V_c$ is based on standard finite element polynomials, representing coarse-scale solution that is resolved by the mesh. $p_f \in V_f$ is an enhancement or enrichment, representing fine or subgrid scale solution. Likewise, the Dirichlet boundary condition (2) is assumed satisfied *ab initio* by the trial solution P_c . Therefore, the fine-scale functions are chosen such that they vanish on the global boundary Γ and satisfy the following system

$$\begin{cases} -\nabla^2(p_c + p_f) - k^2(p_c + p_f) = f & \text{in } \Omega \\ p_f = 0 & \text{on } \Gamma \end{cases} \quad (15)$$

The definition in Eq. (15) justifies the name ‘‘global residual-free’’ in this paper for the enrichments in the oscillatory type of fine-scale approximations as will be described in the next section. Using a simple algebra can help show that the proposed formulation is residual-based in the sense that if the coarse-scale solution is also the exact solution, i.e.,

$$-\nabla^2(p_c) - k^2(p_c) = f \quad \text{in } \Omega \quad (16)$$

then

$$p_f = 0 \quad \text{in } \Omega, \quad (17)$$

thus the fine-scale vanishes identically.

Substituting Eqs. (12) and (14) into Eq. (6) and exploiting the linearity of the test function slot we can split Eq. (6) into a coarse-scale and a fine-scale problem. The application of Green’s theorem and cancellation of surface terms lead to equations consist of the coarse-scale equation

$$\begin{aligned} & \int_{\Omega} \nabla w_c \cdot \nabla(p_c + p_f) d\Omega - k^2 \int_{\Omega} w_c(p_c + p_f) d\Omega + i\rho\omega A_n \int_{\Gamma_B} w_c(p_c) d\Gamma \\ & = \int_{\Omega} f w_c d\Omega - i\rho\omega \int_{\Gamma_N} w_c v_n d\Gamma \quad \forall w_c \in V_c \end{aligned} \quad (18)$$

or

$$A(w_c, p_c) + A(w_c, p_f) + i\rho\omega A_n(w_c, p_c)_{\Gamma_B} = (w_c, f)_{\Omega} - i\rho\omega(w_c, v_n)_{\Gamma_N} \quad \forall w_c \in V_c \quad (19)$$

and the fine-scale equation

$$\int_{\Omega} \nabla w_f \cdot \nabla(p_c + p_f) d\Omega - k^2 \int_{\Omega} w_f(p_c + p_f) d\Omega = \int_{\Omega} f w_f d\Omega \quad \forall w_f \in V_f \quad (20)$$

or

$$A(w_f, p_c) + A(w_f, p_f) = (w_f, f)_{\Omega} \quad \forall w_f \in V_f \quad (21)$$

Note the boundary terms in Eq. (20) drop out in the fine-scale equation because of the space chosen for the fine-scale approximation.

The general idea at this point is to solve Eq. (20) and extract the expression for the fine-scale field. The expression then can be substituted in the coarse-scale equation defined by Eq. (19), thereby eliminating the explicit presence of the fine-scale field, yet modeling its effect. In standard VMS method using the fine-scale Green’s function, the sesquilinear forms $A(w_f, p_c)$ and $A(w_f, p_f)$ in Eq. (21) are further expressed using integration by parts and Eq. (15) to yield

$$\begin{aligned}
 A(w_f, p_c) &= (w_f, \Theta p_c)_{\Omega'} + (w_f, \llbracket \mathbf{n}_e \cdot \nabla p_c \rrbracket)_{\Gamma'} + (w_f, \mathbf{n}_e \cdot \nabla p_c)_{\Gamma_N + \Gamma_B} \\
 &= (w_f, \Theta p_c)_{\Omega'} + (w_f, \llbracket \mathbf{n}_e \cdot \nabla p_c \rrbracket)_{\Gamma'} \\
 &= (w_f, \Theta p_c)_{\Omega}
 \end{aligned} \tag{22}$$

$$\begin{aligned}
 A(w_f, p_f) &= (w_f, \Theta p_f)_{\Omega'} + (w_f, \llbracket \mathbf{n}_e \cdot \nabla p_f \rrbracket)_{\Gamma'} + (w_f, \mathbf{n}_e \cdot \nabla p_f)_{\Gamma_N + \Gamma_B} \\
 &= (w_f, \Theta p_f)_{\Omega'} + (w_f, \llbracket \mathbf{n}_e \cdot \nabla p_f \rrbracket)_{\Gamma'} \\
 &= (w_f, \Theta p_f)_{\Omega}
 \end{aligned} \tag{23}$$

where $\Omega' = \bigcup_{e=1}^{n_{el}} \Omega_e$ is the union of element interiors, $\Gamma' = \left(\bigcup_{e=1}^{n_{el}} \Gamma_e \right) - \Gamma$ represents the summation of element skeleton. The jump operator $\llbracket \cdot \rrbracket$ is defined by

$$\llbracket \mathbf{n}_e \cdot \mathbf{b} \rrbracket = \mathbf{n}_e \cdot (\mathbf{b}^+ - \mathbf{b}^-) \tag{24}$$

where \mathbf{n}_e denotes a unit normal vector on the element boundary. Θp_c and Θp_f are *Dirac distributions* (Hughes *et al.* 2004) on Ω . Substituting Eqs. (22) and (23) into Eq. (21) leads to the following fine-scale equation

$$(w_f, \Theta p_c)_{\Omega} + (w_f, \Theta p_f)_{\Omega} = (w_f, f)_{\Omega} \quad \forall w_f \in V_f = \bigoplus_{\Omega_e} H_0^1(\Omega_e) \tag{25}$$

which can be used to solve the Green's function problem (see e.g. Oberai and Pinsky 1998 for details). By assuming zero Dirichlet boundary conditions on every element boundary for element Green's function together with the homogenous boundary condition in Eq. (17), the local fine-scale solution can be obtained by

$$\begin{aligned}
 p_f(\mathbf{x}_0) &= - \int_{\Omega} g'(\mathbf{x}, \mathbf{x}_0) (\Theta p_c - f)(\mathbf{x}) d\Omega_x \\
 &= - \int_{\Omega'} g'(\mathbf{x}, \mathbf{x}_0) (\Theta p_c - f)(\mathbf{x}) d\Omega_x - \int_{\Gamma'} g'(\mathbf{x}, \mathbf{x}_0) \llbracket \mathbf{n}_e \cdot \nabla p_c \rrbracket(\mathbf{x}) d\Gamma_x \\
 &\approx - \int_{\Omega'} g'_e(\mathbf{x}, \mathbf{x}_0) (\Theta p_c - f)(\mathbf{x}) d\Omega_x - \int_{\Gamma'} g'_e(\mathbf{x}, \mathbf{x}_0) \llbracket \mathbf{n}_e \cdot \nabla p_c \rrbracket(\mathbf{x}) d\Gamma_x \\
 &= - \sum_{e=1}^{n_{el}} \left(\int_{\Omega_e} g'_e(\mathbf{x}, \mathbf{x}_0) (\Theta p_c - f)(\mathbf{x}) d\Omega_x + \int_{\Gamma_e} g'_e(\mathbf{x}, \mathbf{x}_0) \llbracket \mathbf{n}_e \cdot \nabla p_c \rrbracket(\mathbf{x}) d\Gamma_x \right) \\
 &= - \sum_{e=1}^{n_{el}} \int_{\Omega_e} g'_e(\mathbf{x}, \mathbf{x}_0) (\Theta p_c - f)(\mathbf{x}) d\Omega_x
 \end{aligned} \tag{26}$$

where $g'(\mathbf{x}, \mathbf{x}_0)$ is the global fine-scale Green's function for a kind of interior Helmholtz equation with homogeneous boundary conditions evaluated at \mathbf{x}_0 . $g'_e(\mathbf{x}, \mathbf{x}_0)$ is the element-wise approximation of Green's function. It is clear that Eq. (26) has lost the global effects due to the restriction of element Green's function to a vanishing trace on the element boundaries. In order to retrieve the global effects on the fine-scale approximations, a global fine-scale approximation

constructed using meshfree method is considered in this study. Note that since global Green's functions are only known for relatively simple configurations, we are not using Green's functions for the global fine-scale approximations in general cases. In the content of VMS method, w_c and p_c take the form

$$w_c(\mathbf{x}) = N(\mathbf{x})\mathbf{W}_c \Rightarrow \nabla w_c = \nabla N(\mathbf{x})\mathbf{W}_c \quad (27)$$

$$p_c(\mathbf{x}) = N(\mathbf{x})\mathbf{P}_c \Rightarrow \nabla p_c(\mathbf{x}) = \nabla N(\mathbf{x})\mathbf{P}_c \quad (28)$$

where $N(\mathbf{x})$ is the finite element shape function in row vector, while $\mathbf{P}_c = [p_c^1 \ p_c^2 \ \dots]^T$ is the discretized field variable in column vector that needs to be determined and $\mathbf{W}_c = [w_c^1 \ w_c^2 \ \dots]^T$ is its variation. Similarly for the global fine-scale approximations and their gradients, we have

$$w_f(\mathbf{x}) = \boldsymbol{\varphi}(\mathbf{x})\mathbf{W}_f \Rightarrow \nabla w_f(\mathbf{x}) = \nabla \boldsymbol{\varphi}(\mathbf{x})\mathbf{W}_f \quad (29)$$

$$p_f(\mathbf{x}) = \boldsymbol{\varphi}(\mathbf{x})\mathbf{P}_f \Rightarrow \nabla p_f(\mathbf{x}) = \nabla \boldsymbol{\varphi}(\mathbf{x})\mathbf{P}_f \quad (30)$$

where $\boldsymbol{\varphi}(\mathbf{x})$ is the shape function of global fine-scale approximations in row vector and its derivation will be described in the next section. $\mathbf{P}_f = [p_f^1 \ p_f^2 \ \dots]^T$ is the unknown discretized field variable with its variation $\mathbf{W}_f = [w_f^1 \ w_f^2 \ \dots]^T$. Substituting Eqs. (29) and (30) into Eq. (25) and invoking the arbitrariness of \mathbf{W}_f leads to

$$\mathbf{K}_{ff}\mathbf{P}_f = \bar{\mathbf{R}} \quad (31)$$

where \mathbf{K}_{ff} is the coefficient matrix which is symmetric, and $\bar{\mathbf{R}}$ is right-hand side term that is related to the residuals from the homogeneous coarse-scale solution and the effect from the source term. They are defined by

$$\mathbf{K}_{ff} = \left(\int_{\Omega} \nabla \boldsymbol{\varphi}(\mathbf{x})^T \nabla \boldsymbol{\varphi}(\mathbf{x}) d\Omega - k^2 \int_{\Omega} \boldsymbol{\varphi}(\mathbf{x})^T \boldsymbol{\varphi}(\mathbf{x}) d\Omega \right) \quad (32)$$

$$\bar{\mathbf{R}} = \mathbf{F}_f - \mathbf{K}_{fc}\mathbf{P}_c \quad (33)$$

$$\mathbf{F}_f = \int_{\Omega} f\boldsymbol{\varphi}(\mathbf{x}) d\Omega \quad (34)$$

$$\mathbf{K}_{fc} = \left(\int_{\Omega} \nabla \boldsymbol{\varphi}(\mathbf{x})^T \nabla N(\mathbf{x}) d\Omega - k^2 \int_{\Omega} \boldsymbol{\varphi}(\mathbf{x})^T N(\mathbf{x}) d\Omega \right) \quad (35)$$

Similarly, we have the following linear system for coarse-scale solution

$$\mathbf{K}_{cc}\mathbf{P}_c = \bar{\bar{\mathbf{R}}} \quad (36)$$

where \mathbf{K}_{cc} represents the standard symmetric coefficient matrix interpolated by the low-order finite elements. Right-hand side term $\bar{\mathbf{R}}$ includes the original right-hand side term \mathbf{F}_c from the coarse-scale and an additional term contributed from the fine-scale solution. They are given by

$$\mathbf{K}_{cc} = \left(\int_{\Omega} \nabla N(\mathbf{x})^T \nabla N(\mathbf{x}) d\Omega - k^2 \int_{\Omega} N(\mathbf{x})^T N(\mathbf{x}) d\Omega + i\rho\omega A_n \int_{\Gamma_B} N(\mathbf{x})^T N(\mathbf{x}) d\Gamma \right) \quad (37)$$

$$\bar{\mathbf{R}} = \mathbf{F}_c - \mathbf{K}_{cf} \mathbf{P}_f \quad (38)$$

$$\mathbf{F}_c = \int_{\Omega} f N(\mathbf{x}) d\Omega - i\rho\omega \int_{\Gamma_N} N(\mathbf{x}) v_n d\Gamma \quad (39)$$

$$\mathbf{K}_{cf} = \left(\int_{\Omega} \nabla N(\mathbf{x})^T \nabla \varphi(\mathbf{x}) d\Omega - k^2 \int_{\Omega} N(\mathbf{x})^T \varphi(\mathbf{x}) d\Omega \right) = \mathbf{K}_{fc}^T \quad (40)$$

The combination of (31) and (36) yields a linear equation solving for coarse-scale and fine-scale solutions.

$$\begin{bmatrix} \mathbf{K}_{cc} & \mathbf{K}_{fc}^T \\ \mathbf{K}_{fc} & \mathbf{K}_{ff} \end{bmatrix} \cdot \begin{bmatrix} \mathbf{P}_c \\ \mathbf{P}_f \end{bmatrix} = \begin{bmatrix} \mathbf{F}_c \\ \mathbf{F}_f \end{bmatrix} \quad (41)$$

Since fine-scale approximations satisfy the homogenous boundary condition, the fine-scale nodal coefficients associated with the boundary nodes become null. Accordingly, the vector \mathbf{P}_f contains only the node set of interior nodes. Eq. (41) can also be written in a condensed form

$$(\hat{\mathbf{K}}) \mathbf{P}_c = \hat{\mathbf{R}} \quad (42)$$

where

$$\hat{\mathbf{K}} = \mathbf{K}_{cc} - \mathbf{K}_{fc}^T \mathbf{K}_{ff}^{-1} \mathbf{K}_{fc} \quad (43)$$

$$\hat{\mathbf{R}} = \mathbf{F}_c - \mathbf{K}_{fc}^T \mathbf{K}_{ff}^{-1} \mathbf{F}_f \quad (44)$$

Now the new coefficient matrix $\hat{\mathbf{K}}$ remains symmetric, and it contains the low-scale coefficient matrix \mathbf{K}_{cc} and a stabilization term $\mathbf{K}_{fc}^T \mathbf{K}_{ff}^{-1} \mathbf{K}_{fc}$ from the fine-scale approximations. Note that fine-scale approximations reside completely in the definition of the stabilization term. Accordingly, the positive-definite system of the final Eq. (42), and thus the discrete analogue of ellipticity of the Helmholtz equation is controlled by the characteristics of the fine-scale approximations.

4. Fine-scale approximations

In this section, the global fine-scale approximations are constructed using the wave-based meshfree approximations to capture the oscillatory type of fine-scale solution. The fine-scale

equation of Eq. (25) can be re-expressed in the following residual form

$$\left(w_f, \Theta p_f \right)_\Omega = \left(w_f, f - \Theta p_c \right)_\Omega \quad \forall w_f \in V_f \quad (45)$$

The corresponding strong form (Euler-Lagrangian equation) to Eq. (45) is

$$\begin{cases} \Theta p_f = f - \Theta p_c & \text{in } \Omega \\ p_f = 0 & \text{on } \Gamma \end{cases} \quad (46)$$

with relevant Green's function problem defined by

$$\begin{cases} \Theta g'(\mathbf{x}, \mathbf{x}_0) = \delta(\mathbf{x} - \mathbf{x}_0) & \text{in } \Omega \\ g'(\mathbf{x}, \mathbf{x}_0) = 0 & \text{on } \Gamma \end{cases} \quad (47)$$

Since the operator Θ is linear, the fine-scale solution of Eq. (46) can be determined in terms of global Green's function given by

$$p_f(\mathbf{x}_0) = - \int_\Omega g'(\mathbf{x}, \mathbf{x}_0) (\Theta p_c - f)(\mathbf{x}) d\Omega_x \quad (48)$$

Note Eq. (48) is a theoretically exact formulation for p_f and the problem of Eq. (46) lies in finding the Green's function g' that satisfies Eq. (47).

On the other hand, the proposed global fine-scale approximations in Eq. (31) can also be written by

$$\mathbf{P}_f = -\mathbf{K}_{ff}^{-1} \left(\mathbf{K}_{ft} \mathbf{P}_c - \mathbf{F}_f \right) \quad (49)$$

Compare Eq. (49) to Eq. (48), we can observe the matrix \mathbf{K}_{ff}^{-1} in Eq. (49) plays a role like the global fine-scale Green's function $g'(\mathbf{x}, \mathbf{x}_0)$. The main numerical issue in constructing the global fine-scale approximations using meshfree method is the satisfaction of $p_f = 0$ on Γ . To solve this numerical issue, the wave-based approximations generated by the Generalized Meshfree (GMF) convex approximation are employed to obtain the global fine-scale approximations.

The fundamental idea of the GMF approximation (Wu *et al.* 2011) is the introduction of an enriched basis function in the Shepard function to achieve linear consistency. The choice of the basis function determines whether the GMF approximation has convexity property and if the corresponding global fine-scale approximations satisfy $p_f = 0$ on Γ . In this paper, a convex GMF approximation constructed using an exponential basis function is considered. Assume a convex hull $\text{conv}(\Lambda)$ of a node set $\Lambda = \{\mathbf{x}_i, i = 1, \dots, n\} \subset \mathbb{R}^2$ defined by (Wu *et al.* 2011)

$$\text{conv}(\Lambda) = \left\{ \sum_{i=1}^n \alpha_i \mathbf{x}_i \mid \mathbf{x}_i \in \Lambda, \alpha_i \in \mathbb{R}, \alpha_i \geq 0, \sum_{i=1}^n \alpha_i = 1, i = 1, 2, \dots \right\}. \quad (50)$$

The GMF method is to construct convex approximations of a given function p in the form

$$p^h(\mathbf{x}) = \sum_{i=1}^n \varphi_i(\mathbf{x}) p^i \quad (51)$$

with the generating function $\varphi_i : \mathbf{conv}(\Lambda) \rightarrow \mathbb{R}$ satisfying the following polynomial reproduction property

$$\sum_{i=1}^n \varphi_i(\mathbf{x}) \mathbf{x}_i = \mathbf{x} \quad \forall \mathbf{x} \in \mathbf{conv}(\Lambda). \quad (52)$$

The first-order GMF approximation in two-dimensions is expressed as

$$\varphi_i(\mathbf{x}) \equiv \varphi_i^a(\mathbf{x}, \lambda_r) = \frac{\kappa_i}{\kappa} = \frac{\phi_a(\mathbf{x}; \mathbf{x} - \mathbf{x}_i) B_i(\mathbf{x} - \mathbf{x}_i, \lambda_r)}{\sum_{j=1}^n \phi_a(\mathbf{x}; \mathbf{x} - \mathbf{x}_j) B_j(\mathbf{x} - \mathbf{x}_j, \lambda_r)} \quad (53)$$

subjected to linear constraints

$$\Xi_r(\mathbf{x}, \lambda_r) = \sum_{i=1}^n \varphi_i^a \cdot (\mathbf{x} - \mathbf{x}_i) = \mathbf{0}, \quad (54)$$

where

$$\kappa_i = \phi_a(\mathbf{x}; \mathbf{x} - \mathbf{x}_i) B_i(\mathbf{x} - \mathbf{x}_i, \lambda_r), \quad (55)$$

$$\kappa = \sum_{i=1}^n \kappa_i = \sum_{i=1}^n \phi_a(\mathbf{x}; \mathbf{x} - \mathbf{x}_i) B_i(\mathbf{x} - \mathbf{x}_i, \lambda_r), \quad (56)$$

The notation $\phi_a(\mathbf{x}; \mathbf{X}_i)$ in Eq. (53) represents the weight function of node i with support size $\text{supp}(\phi_a(\mathbf{x}; \mathbf{x} - \mathbf{x}_i)) = a_i$. $B_i(\mathbf{x} - \mathbf{x}_i, \lambda_r)$ denotes the basis function of the GMF approximation. \mathbf{x} is the coordinate of material point and \mathbf{x}_i is the coordinate of material point evaluated at node i . The symbol n in summations denotes the number of nodes within the support size $a(\mathbf{x})$ at fixed \mathbf{x} . $\lambda_r(\mathbf{x})$ ($r = 2$) are the constraint parameters which have to be determined.

In the GMF approximation, the property of the partition of unity is automatically satisfied by the normalization in Eq. (53). The completion of the GMF approximation is achieved by finding λ to satisfy Eq. (54). To determine λ at any fixed \mathbf{x} in Eq. (53), a root-finding algorithm is required for the non-linear basis functions. In this study the Newton-Raphson method is adopted for the equation solving of the objection function in Eq. (54). The partial derivative of the objection function with respect to λ is

$$\mathbf{J} = \sum_{i=1}^n \left[\left(\frac{\phi_a B_{i, \lambda_r}}{\kappa} \right) \otimes (\mathbf{x} - \mathbf{x}_i) \right] - \Xi_r \otimes \sum_{j=1}^n \left(\frac{\phi_a B_{j, \lambda_r}}{\kappa} \right), \quad (57)$$

where \mathbf{J} is a 2×2 Jacobian matrix and \otimes indicates the dyadic product of vectors. Once the converged λ is obtained, the basis functions are computed and the spatial derivative of the GMF

approximation can be obtained and given by

$$\nabla \varphi_i^a = \varphi_{i,\mathbf{x}}^a + \varphi_{i,\lambda}^a \lambda_{r,\mathbf{x}} \quad (58)$$

where

$$\varphi_{i,\mathbf{x}}^a = \frac{\kappa_{i,\mathbf{x}}}{\kappa} - \varphi_i^a \sum_{j=1}^n \frac{\kappa_{j,\mathbf{x}}}{\kappa} \quad (59)$$

$$\kappa_{i,\mathbf{x}} = \phi_{a,\mathbf{x}} B_i + \phi_a B_{i,\mathbf{x}} \quad (60)$$

$$\varphi_{i,\lambda}^a = \frac{\phi_a B_{i,\lambda_r}}{\kappa} - \varphi_i^a \sum_{j=1}^n \left(\frac{\phi_a B_{j,\lambda_r}}{\kappa} \right) \quad (61)$$

$$B(\mathbf{x}, \lambda) = \exp(\mathbf{x}\lambda) \quad (62)$$

$$\lambda_{r,\mathbf{x}} = -\mathbf{J}^{-1} \Xi_{r,\mathbf{x}} \quad (63)$$

$$\Xi_{r,\mathbf{x}} = \sum_{i=1}^n \varphi_{i,\mathbf{x}}^a(\mathbf{x}) + \sum_{i=1}^n \varphi_i^a(\mathbf{x}) = \sum_{i=1}^n \varphi_{i,\mathbf{x}}^a(\mathbf{x}) + 1 \quad (64)$$

A cubic spline function with a rectangular support is chosen to be the weight function in Eq. (55). Finally, the global fine-scale approximations for Eq. (30) can be expressed by

$$p_f(\mathbf{x}) = \sum_{i=1}^n \varphi_i^a p_f^i \quad (65)$$

where p_f^i denotes the fine-scale coefficient of node i . Same fine-scale approximations are applied to Eq. (29). The constructed fine-scale approximations generate the desired weak Kronecker-delta property (Wu and Koishi 2009) with vanishing value on the global boundary. Fig. 1 illustrates one of the fine-scale approximations that satisfy the homogenous Dirichlet boundary condition in Eq. (15).

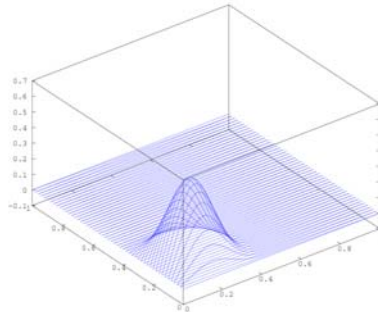


Fig. 1 Illustration of one fine-scale approximation

Table 1 Three formulations adopted in the numerical comparison

Name	Description
FEML	4-noded bilinear finite element formulation (2-noded in 1D).
FEMQ	8-noded quadratic finite element formulation (3-noded in 1D).
PRESENT	Multi-scale meshfree-enriched finite element formulation.

5. Numerical examples

In this section, two benchmark examples are analyzed to study the performance of the present method for the multi-scale analysis of acoustic wave propagation problems. The normalized nodal support size in Eq. (53) for the global fine-scale approximations is chosen to be 3.0 for all numerical examples. A four-point Gauss quadrature rule is employed for the integration of discrete equations in Eq. (42). As comparison, we also provide the results from the bilinear and quadratic finite element formulations. A list of abbreviations for those methods along with their brief descriptions is given in Table 1. Unless otherwise specified, dimensionless unit system is adopted in this paper for convenience.

5.1 Wave propagation in bar

The one-dimension wave propagation in frequency domain is investigated. Same problem has been studied in (Uras *et al.* 1997) using Reproducing Kernel Particle Method (RKPM). The 1D waveguide has a length of 10 and is uniformly discretized into 20 elements using piece-wise linear finite elements or 10 elements using quadratic finite elements. This discretization corresponds to 21 nodes for all three numerical methods. The governing equation for this problem can be described by the following Helmholtz equation

$$-\nabla^2 p - k^2 p = f(x) \text{ in } \Omega. \tag{66}$$

Two cases are examined in this 1D example:

- (1) The first case considers a homogenous differential equation with non-homogenous boundary condition described by

$$f(x) = 0, p(0) = 1 \text{ and } p(10) = 0. \tag{67}$$

The analytical solution of this case is given by

$$p(x) = \frac{\sin(k(10-x))}{\sin(10k)}. \tag{68}$$

Figs. 2(a)-(c) compares the results with three different wave numbers, $k = 2, 3, 4$ using evenly-distributed nodes. It can be seen that linear FEM experiences large amplitude error even with $k = 2$ which corresponds to five elements per wavelength in this example. The large amplitude error in linear FEM is related to the approximation error. On the other hand, the presence of pollution error in linear FEM can be verified by increasing wave number k as shown in

Fig. 2(b). Severe pollution error is observed in the case $k = 4$, and thus is not plotted in Fig. 2(c). Quadratic FEM improves the solution of linear FEM in particular for the case with a higher wave number. However, the improvement is limited to the resolution of mesh in higher-order elements as shown in Fig. 2(c). The present multi-scale approach achieves a good agreement with analytical solution for all three different wave numbers. Particularly in Fig. 2(c), the present method demonstrates an excellent ability to model the short wavelengths. When $k = 4$, only 3 elements (2 elements for Nyquist limit) per wavelength are required in the present method to meet the analytical solution.

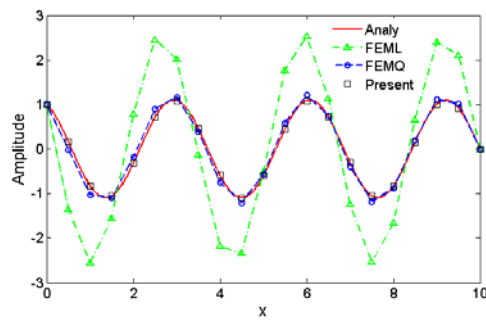
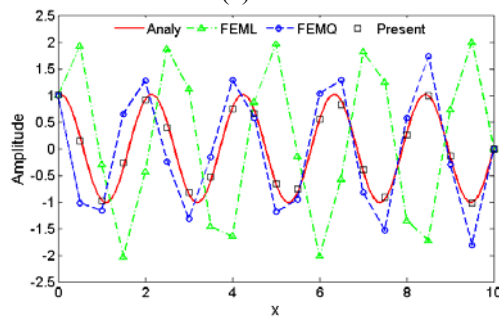
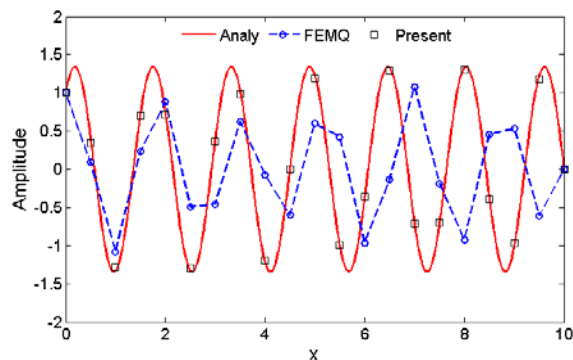
(a) $k = 2$ (b) $k = 3$ (c) $k = 4$

Fig. 2 Comparison of solution in different wave numbers using regular mesh (1st case)

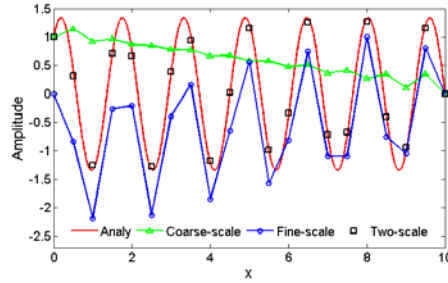
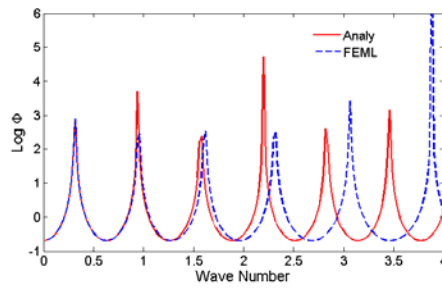
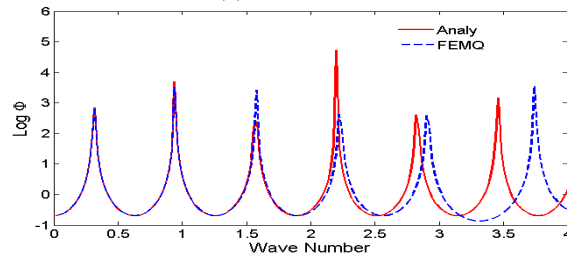


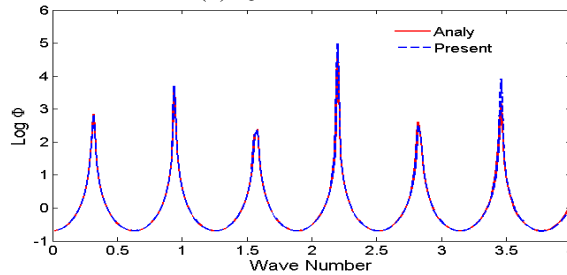
Fig. 3 The components of coarse and fine scale in two-scale solution with $k = 4$ (1st case)



(a) Linear FEM

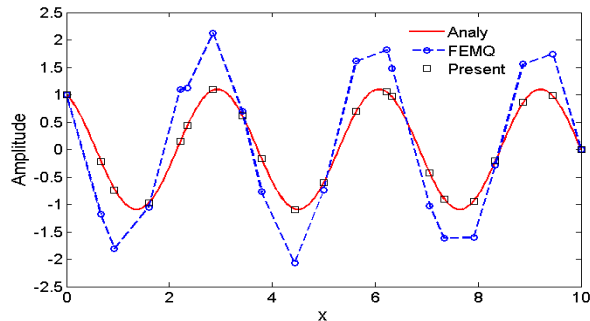
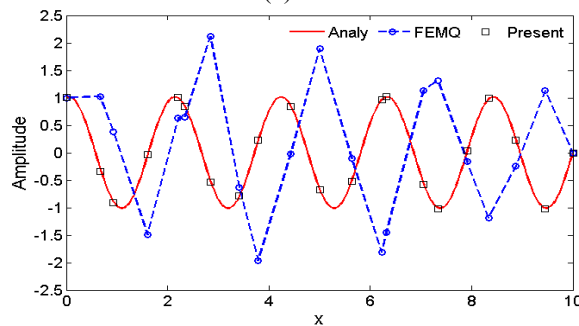
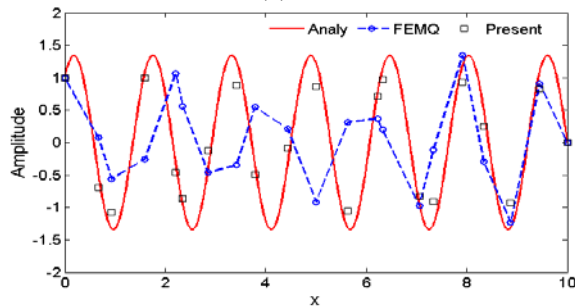


(b) Quadratic FEM



(c) Present multi-scale method

Fig. 4 Swept spectrum analyses with wave number $\in (0, 4]$ using regular mesh (1st case)

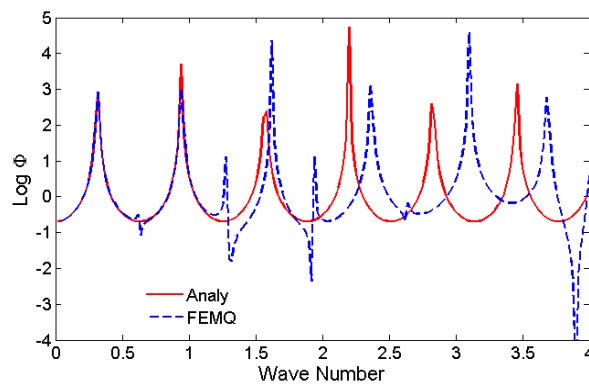
(a) $k = 2$ (b) $k = 3$ (c) $k = 4$ Fig. 5 Comparison of solution in different wave numbers using irregular mesh (1st case)

The coarse and fine scale components of the present multi-scale method for wave number $k = 4$ are plotted in Fig. 3. The coarse solution in Fig. 3 presents a relatively smooth solution that is interpolated by the linear finite element method. The fine-scale component is a nonlocal solution which is approximated by the global residual-free meshfree enrichment. The fine-scale solution satisfies the homogenous Dirichlet boundary in Eq. (15) as shown in Fig. 3 and offers the ability to reduce the pollution error in the highly oscillated wave solution that is outside the discretization level.

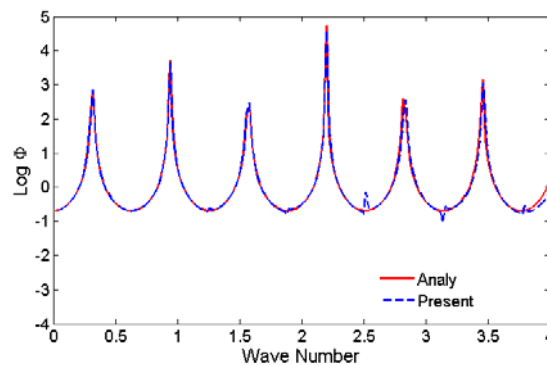
Superior performance of the present method over two other methods can also be seen in Figs. 4(a)-(c). Figs. 4(a)-(c) compare the middle point displacement between the analytical and

numerical solution where the wave number varies from zero to 4. The results of linear and quadratic FEM methods show good agreements for low wave numbers, but have significant deteriorations for high wave numbers. The result of the present method matches the analytical solution very well in all spectrums. The present method also improves the RKPM solution for the shorter waves as presented in Fig. 6 of (Uras *et al.* 1997).

The sensitivity of mesh irregularity to the wave solution is also studied in this example. Since the solution of linear FEM deteriorates significantly in this test example, its result is therefore omitted and not reported in this paper. The results of quadratic FEM are shown in Figs. 5(a)-(c). The performance of quadratic FEM using irregular nodal distribution is much worse than the one using regular mesh as illustrated in Figs. 5(a)-(c). Remarkably, the present method with the irregular discretization maintains the same accuracy level as in the case of regular mesh for low wave number and outperforms the quadratic FEM for high wave number as depicted in Fig. 5(c). Consistent result is observed in Figs. 6(a)-(b) which compare the middle point displacement with wave number ranging from zero to four. In this study, we observe a poor performance of linear and quadratic FEM methods when mesh becomes irregular.



(a)



(b)

Fig. 6 Swept spectrum analyses using irregular mesh (1st case)

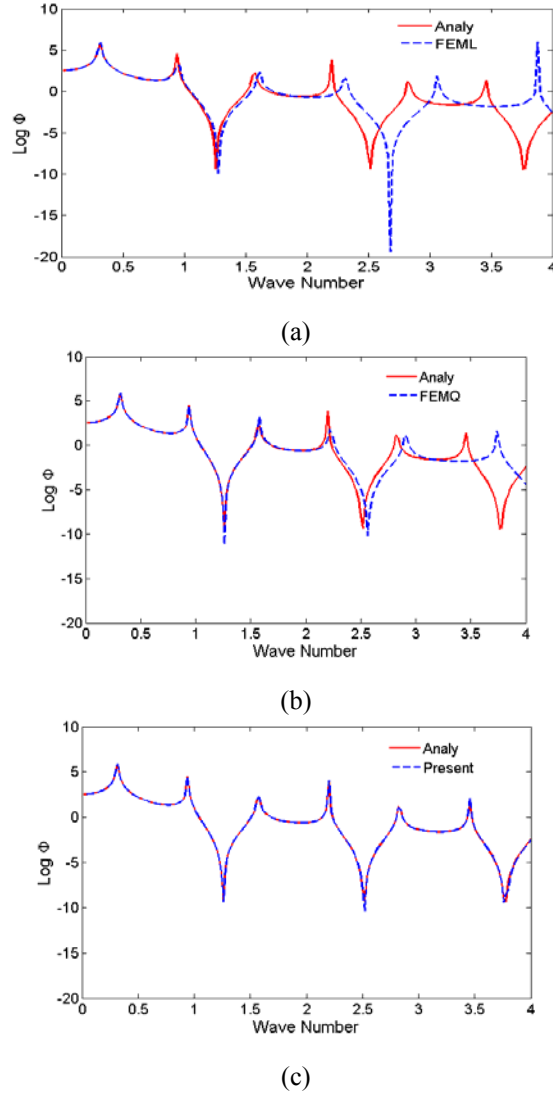


Fig. 7 Swept spectrum analyses using regular mesh (2nd case)

(2) The second case considers a nonhomogenous differential equation with homogenous boundary condition, with $f(x) = 1$. The analytical solution of this case is given by

$$p(x) = \frac{1}{k^2} \left[1 - \cos(kx) + \frac{\cos(10k) - 1}{\sin(10k)} \sin(kx) \right]. \quad (69)$$

Fig. 7 depicts the comparison of the middle point displacement between the analytical and numerical solution using regular mesh. Similar to the results in Case (1), the present method in this case yields much more accurate results over linear and quadratic FEM in the wave number

spectrum analysis especially in high wave numbers. We can conclude from this numerical study that meshfree enrichment to the unresolved fine scales in VMS method allows FEM to effectively approximate high wave number problem that is beyond the mesh resolution.

5.2 The acoustic square domain problem with robin boundary conditions

The effectiveness of the present method in two-dimension case is examined in this plane wave propagation problem. The standard FEM method usually is sensitive to the mesh orientation relative to the plane wave propagation direction which is generally not known *a priori* in real problems. The problem in this example is taken from (Bouillard and Suleau 1998, Yao *et al.* 2010) which considers a unit square domain with Robin boundary conditions prescribed on all four edges under different plane wave propagation directions. The governing equation for this problem can be described by the following Helmholtz equation

$$\begin{aligned} -\nabla^2 p - k^2 p &= 0 \quad \text{in } \Omega \\ p &= 1 \quad \text{at } x = 0, y = 0 \end{aligned} \quad (70)$$

with non-homogenous Robin boundary conditions as follows

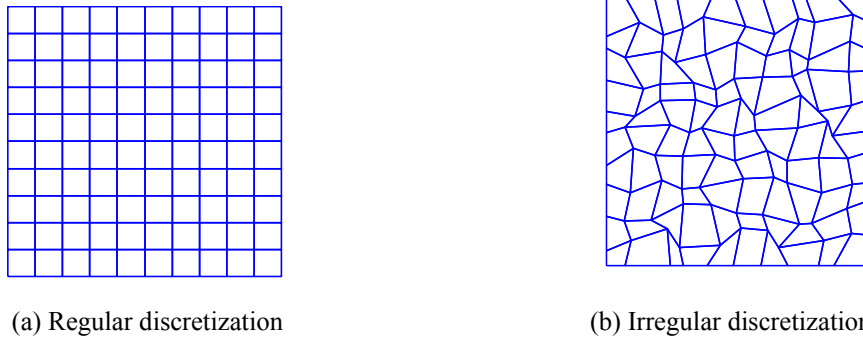
$$\nabla p \cdot \mathbf{n} = \begin{cases} -ikp \cos \beta & x = 0 \\ +ikp \cos \beta & x = 1 \\ -ikp \sin \beta & y = 0 \\ +ikp \sin \beta & y = 1 \end{cases} \quad (71)$$

The analytical solution of this problem is a plane wave propagating along a direction inclined with an angle of β degrees on x-axis and is given by

$$p(x, y) = \cos[k(x \cos \beta + y \sin \beta)] + i \sin[k(x \cos \beta + y \sin \beta)]. \quad (72)$$

The regular and irregular 10×10 discretization are used, as shown in Fig. 8. Since the Robin boundary conditions (RBC) in this problem are highly oscillated for high wave number and only satisfied by the coarse-scale solution in the weak sense, the residual of RBC is introduced in the fine-scale equation and minimized using the present variational multi-scale framework.

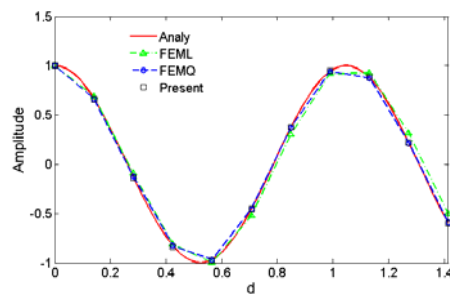
Figs. 9(a)-(c) show the real part of the solution by three comparing methods under different wave number k and RBC parameter β using a regular discretization. For the case of $k = 6$ and $\beta = \pi/4$, all three numerical methods generate the solutions which are in good agreements with the analytical solution as depicted in Fig. 9(a). Linear FEM solution loses the accuracy significantly as wave number increases to be $k = 12$ as shown in Fig. 9(b). The sensitivity of pollution error to the wave propagation direction is investigated and reported in Fig. 9(c) using $k = 12$. When the dominant direction of propagation becomes $\beta = \pi/24$, both linear and quadric FEM produce notorious pollution error as presented in Fig. 9(c). In contrast, the present method demonstrates its superiority over FEM in minimizing the pollution error even when the fine-scale approximations do not contain the information of plane wave propagation direction.



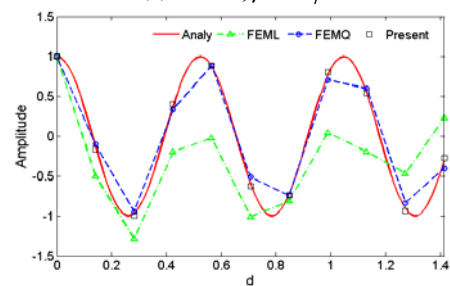
(a) Regular discretization

(b) Irregular discretization

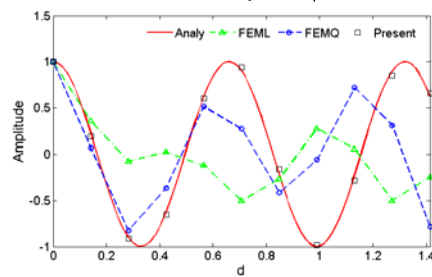
Fig. 8 Discretization in acoustic wave problem with Robin boundary condition



(a) $k = 6, \beta = \pi/4$



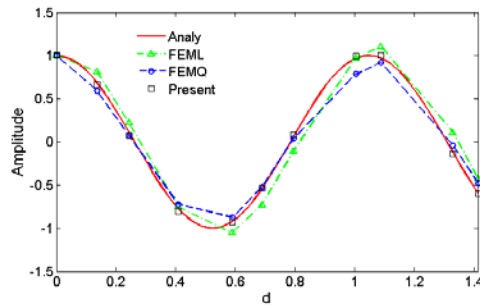
(b) $k = 12, \beta = \pi/4$



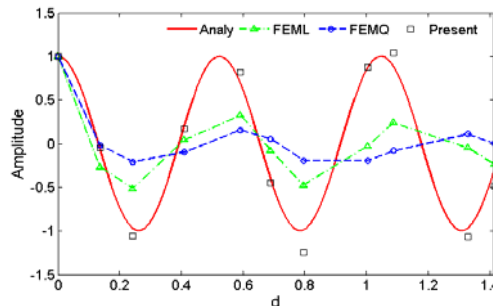
(c) $k = 12, \beta = \pi/24$

Fig. 9 Comparison of real part solution using regular mesh

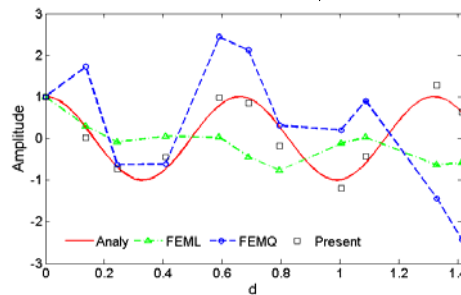
When mesh becomes irregular, large error is observed in both linear FEM and quadratic FEM methods as depicted in Figs. 10(a)-(c). Strong mesh dependence in FEM solution can be observed by comparing Fig. 9(b) and Fig. 10(b). The pollution error increases dramatically for linear and quadratic FEM when the plane wave is oriented at an angle of $\beta=\pi/24$ as shown in Fig. 10(c). While FEM suffers from accuracy deterioration in irregular discretization, the present method is able to retain its superior performance, albeit to a lesser degree, when mesh is irregular and in different wave propagation directions. Results of this numerical example indicate that the global meshfree enrichments in VMS method substantially improve the accuracy of single-scale FEM method that is prominently sensitive to the mesh orientation and wave propagation direction in the two-dimensional acoustic wave analysis.



(a) $k = 6, \beta = \pi/4$



(b) $k = 12, \beta = \pi/4$



(c) $k = 12, \beta = \pi/24$

Fig. 10 Comparison of real part solution using irregular mesh

6. Conclusions

We have presented a general framework for the global residual-free meshfree enrichment in the multi-scale finite element formulation. In this study, the present meshfree-enriched multi-scale finite element formulation is applied to the acoustic wave propagation problems. The fine-scale approximations in the present method are generated from the meshfree convex approximations constructed by the Generalized Meshfree approximation, and thus maintain the continuity of fine-scale fluxes across the finite element boundaries and do not require a complicated treatment on the jump terms. Since the global wave pattern is not incorporated in the fine-scale basis functions, no *a priori* knowledge of fundamental solution in the fine-scale approximation is assumed. The present multi-scale variational decoupling of the Helmholtz equation facilitates accurate modeling of acoustic waves at different scales as demonstrated in the numerical examples. The extension of the formulation to the exterior Helmholtz equation as well as other PDEs is under developing and will be presented in the near future.

Acknowledgements

The authors wish to thank Dr. John O. Hallquist of LSTC for his support to this research.

References

- Babuska, I., Ihlenburg, F., Paik, E. and Sauter, S. (1995), "A generalized finite element method for solving the Helmholtz equation in two dimensions with minimal pollution", *Comput. Meth. Appl. M.*, **128**(3-4), 325-359.
- Baiges, J. and Codina, R. (2013), "A variational multiscale method with subscales on the element boundaries for the Helmholtz equation", *Int. J. Numer. Meth. Eng.*, **93**(6), 664-684.
- Belytschko, T. and Mullen, R. (1978), "On dispersive properties of finite element solutions", *Modern Problems in Elastic Wave Propagation*, John Wiley & Sons, Ltd.
- Belytschko, T., Lu, Y.Y. and Gu, L. (1994), "Element-free Galerkin methods", *Int. J. Numer. Meth. Eng.*, **37**(2), 229-256.
- Bouillard, P. and Suleau, S. (1998), "Element-free Galerkin solutions for Helmholtz problems: formulation and numerical assessment of pollution effect", *Comput. Meth. Appl. Mech. Eng.*, **161**, 317-335.
- Franca, L.P., Madureira, A.L. and Valentin, F. (2005), "Towards multiscale functions: enriching finite element spaces with local but not bubble-like functions", *Comput. Meth. Appl. Mech. Eng.*, **194**(27-29), 3006-3021.
- Farhat, C., Harari, I. and Franca, L.P. (2001), "The discontinuous enrichment method", *Comput. Meth. Appl. Mech. Eng.*, **190**, 6455-6479.
- Harari, I. and Hughes, T.J.R. (1991), "Finite element method for the Helmholtz equation in an exterior domain: Model problems", *Comput. Meth. Appl. Mech. Eng.*, **87**(1), 59-96.
- Harari, I. and Hughes, T.J.R. (1992), "Galerkin/least squares finite element method for the reduced wave equation with non-reflecting boundary conditions", *Comput. Meth. Appl. Mech. Eng.*, **98**(3), 441-454.
- Harari, I. and Gosteev, K. (2007), "Bubble-based stabilization for the Helmholtz equation", *Int. J. Numer. Meth. Eng.*, **70**(10), 1241-1260.
- Harari, I. (2008), "Multiscale finite elements for acoustics: continuous, discontinuous, and stabilized methods", *Int. J. Numer. Meth. Eng.*, **6**, 511-531.
- Hu, W., Wu, C.T. and Koishi, M. (2012), "A displacement-based nonlinear finite element formulation using

- meshfree-enriched triangular elements for the two-dimensional large deformation analysis of elastomers”, *Finite Elem. Anal. Des.*, **50**, 161-172.
- Hughes, T.J.R., Scovazzi, G. and Franca, L.P. (2004), “Multiscale and stabilized methods”, *Encyclopedia of Computational Mechanics*, John Wiley & Sons, Ltd, **3**.
- Hughes, T.J.R. and Sangalli, G. (2007), “Variational multiscale analysis: the fine-scale Green’s function, projection, optimization, localization, and the stabilized methods”, *SIAM J. Numer. Anal.*, **45**(2), 539-557.
- Ihlenburg, F. and Babuska, I. (1995), “Finite element solution of the Helmholtz equation with high wave number Part I: The h-version of FEM”, *Comput. Math. Appl.*, **30**(9), 9-37.
- Ihlenburg, F. and Babuska, I. (1997), “Finite element solution of the Helmholtz equation with high wave number Part II: The h-p version of FEM”, *SIAM J. Numer. Anal.*, **34**(1), 315-358.
- Lai, S.J., Wang, B.Z. and Duan, Y. (2010), “Solving Helmholtz equation by meshless radial basis functions method”, *Prog. Electromagnetics Res. B*, **24**, 351-367.
- Liu, W.K., Jun, S. and Zhang, Y.F. (1995), “Reproducing kernel particle methods”, *Int. J. Numer. Meth. Fl.*, **20**(8-9), 1081-1106.
- Liu, W.K., Hao, W., Chen, Y., Jun, S. and Gosz, J. (1997), “Multiresolution reproducing kernel particle methods”, *Comput. Mech.*, **20**, 295-309.
- Oberai, A.A. and Pinsky, P.M. (1998), “A multiscale finite element method for the Helmholtz equation”, *Comput. Meth. Appl. Mech. Eng.*, **154**(3-4), 281-297.
- Oberai, A.A. and Pinsky, P.M. (2000), “A residual-based finite element method for the Helmholtz equation”, *Int. J. Numer. Meth. Eng.*, **49**(3), 399-419.
- Park, C.K., Wu, C.T. and Kan, C.D. (2011), “On the analysis of dispersion property and stable time step in meshfree method using generalized meshfree approximation”, *Finite Elem. Anal. Des.*, **47**(7), 683-697.
- Suleau, S. and Bouillard, P. (2000), “One-dimensional dispersion analysis for the element-free Galerkin method for the Helmholtz equation”, *Int. J. Numer. Meth. Eng.*, **47**(6), 1169-1188.
- Uras, R.A., Chang, C.T., Chen, Y. and Liu, W.K. (1997), “Multi-resolution reproducing kernel particle methods in Acoustics”, *J. Comput. Acoust.*, **5**, 71-94.
- Voth, T.E. and Christon, M.A. (2001), “Discretization errors associated with reproducing kernel methods: one-dimensional domains”, *Comput. Meth. Appl. Mech. Eng.*, **190**(18-19), 2429-2446.
- Wenterodt, C. and von Estorff, O. (2009), “Dispersion analysis of the meshfree radial point interpolation method for the Helmholtz equation”, *Int. J. Numer. Meth. Eng.*, **77**(12), 1670-1689.
- Wu, C.T. and Koishi, M. (2009), “A meshfree procedure for the microscopic analysis of particle-reinforced rubber compounds”, *Interact. Multiscale Mech.*, **2**(2), 129-151.
- Wu, C.T., Park, C.K. and Chen, J.S. (2011), “A generalized approximation for the meshfree analysis of solids”, *Int. J. Numer. Meth. Eng.*, **85**(6), 693-722.
- Wu, C.T. and Hu, W. (2011), “Meshfree-enriched simplex elements with strain smoothing for the finite element analysis of compressible and nearly incompressible solids”, *Comput. Meth. Appl. Mech. Eng.*, **200**(45-46), 2991-3010.
- Wu, C.T., Hu, W. and Chen, J.S. (2012), “A meshfree-enriched finite element method for compressible and near-incompressible elasticity”, *Int. J. Numer. Meth. Eng.*, **90**(7), 882-914.
- Wu, C.T. and Koishi, M. (2012), “Three-dimensional meshfree-enriched finite element formulation for micromechanical hyperelastic modeling of particulate rubber composites”, *Int. J. Numer. Meth. Eng.*, **91**(11), 1137-1157.
- Wu, C.T., Guo, Y. and Askari, E. (2013), “Numerical modeling of composite solids using an immersed meshfree Galerkin method”, *Composit. B*, **45**(1), 1397-1413.
- Yao, L.Y., Yu, D.J., Cui, X.Y. and Zang, X.G. (2010), “Numerical treatment of acoustic problems with the smoothed finite element method”, *Appl. Acoust.*, **71**(8), 743-753.
- You, Y., Chen, J.S. and Voth, T.E. (2002), “Characteristics of semi- and full discretization of stabilized Galerkin meshfree method”, *Finite Elem. Anal. Des.*, **38**(10), 999-1012.